Chapter 2

Modified Finch and Skea stellar model compatible with observational data

In this chapter, we study the physically acceptable stable stellar solutions of Einstein's field equations on the background of a paraboloidal spacetime given by Finch-Skea ansatz [Finch and Skea, 1989]. All the regularity conditions and stability conditions are verified for the observed pulsars and we found that, it matches with the observed masses and radii along with the physical plausibility requirements.

2.1 Introduction

An Ansatz proposed by Duorah and Ray [1987] for the metric potential g_{rr} corresponding to a static spherically symmetric perfect fluid space-time, has been used by Finch and Skea [1989] and they developed a stellar model which was later shown to comply with all the physical requirements of a realistic star by Delgaty and Lake [1998]. Consequently, the Finch-Skea model has been explored by many investigators

in different astrophysical contexts, particularly for the studies of cold compact stellar objects (see for example, Hansraj and Maharaj [2006], Tikekar and Jotania [2009], Banerjee et al. [2013]). One noticeable feature of the Finch-Skea model is that it assumes isotropy in pressure. However, theoretical investigations of Ruderman [1972] and Canuto [1974], amongst others have shown that anisotropy might develop in the high density regime of compact stellar objects. In other words, radial and transverse pressures might not be equal at the interior of ultra-compact stars. Bowers and Liang [1974] have extensively discussed the conditions under which anisotropy might occur at stellar interiors which include presence of type-3A super fluid, electromagnetic field, rotation etc. They have also established the non-negligible effects of local anisotropy on the maximum equilibrium mass and surface redshift of the distribution. Accordingly, different anisotropic stellar models have been developed and effects of anisotropy on physical properties of stellar configurations have been analyzed by many investigators, viz., Maharaj and Maartens [1989], Gokhroo and Mehra [1994], Patel and Mehta [1995], Tikekar and Thomas [1998, 1999, 2005], Thomas et al. [2005], Thomas and Ratanpal [2007]. Impacts of anisotropy on the stability of a stellar configuration have been studied by Dev and Gleiser [2002, 2003, 2004] respectively. Sharma and Maharaj [2007] and Thirukkanesh and Maharaj [2008] have obtained analytic solutions of compact anisotropic stars by assuming a linear equation of state(EOS). To solve the Einstein-Maxwell system, Komathiraj and Maharaj [2007a] have used a linear equation of state. By assuming a linear EOS, Sunzu et al. [2014] have reported solutions for a charged anisotropic quark star. Feroze and Siddiqui [2011] and Maharaj and Takisa [2012] have used a quadratic-type EOS for obtaining solutions of anisotropic distributions. Varela et al. [2010] have analyzed charged anisotropic configurations admitting a linear as well as non-linear equations of state. For a star composed of quark matter in the MIT bag model, Paul et al. [2011] have shown how anisotropy could affect the value of the Bag constant.

For a specific polytropic index, exact solutions to Einstein's field equations for an anisotropic sphere admitting a polytropic EOS have been obtained by Thirukkanesh and Ragel [2012]. Maharaj and Takisa [2013] have used the same type of EOS to develop an analytical model describing a charged anisotropic sphere. Polytropes have also been studied by Nilsson and Uggla [2001], Heinzle et al. [2003] and Kinasiewicz and Mach [2007]. Thirukkanesh and Ragel [2014] have used modified Van der Waals EOS to represent anisotropic charged compact spheres. For specific forms of the gravitational potential and electric field intensity, Malaver [2014] has prescribed solutions for a stellar configuration whose matter content admits a quadratic EOS. Malaver [2013a] and Malaver [2013b] has also found exact solutions to the Einstein-Maxwell system using the Van der Waals modified EOS.

Recently, Sharma and Ratanpal [2013], making use of the Finch and Skea [1989] ansatz, have generated a class of solutions describing the interior of a static spherically symmetric anisotropic star. In this chapter, we have generalized the Sharma and Ratanpal [2013] model by incorporating a dimensionless parameter $n(> 0)$ in the Finch and Skea [1989] ansatz and assumed the system to be anisotropic, in general. We have shown that such assumptions can provide physically viable solutions which can be used to model realistic stars. Implications of the modified ansatz (by including an adjustable parameter n) on the size and physical properties of resultant stellar configurations have been analyzed. Based on physical requirement, we have put constraints on the model parameters and subsequently shown that a wide variety of observed pulsars can be accommodated within the prescribed bound of the model parameters. In particular, we have shown that the predicted masses and radii of pulsars like 4U 1820-30, PSR J1903+327, 4U 1608-52, Vela X-1, PSR J1614-2230, SAX J1808.4-3658 and Her X-1 considered from the exhaustive study carried out by Gangopadhyay et al. [2013] and found that, they all can be well achieved by systematically fixing the parameter n. Most importantly, for a given mass, it is

possible to constrain the radius so as to get the desired compactness by fixing the *compactness parameter* u in this model.

2.2 Modified Finch and Skea model

We write the interior space-time of a static spherically symmetric distribution of anisotropic matter in the form

$$ds^2 = e^{\nu(r)}dt^2 - e^{\lambda(r)}dr^2 - r^2(d\theta^2 + sin^2\theta d\phi^2), \tag{2.1}$$

where,

$$e^{\lambda} = \left(1 + \frac{r^2}{R^2}\right)^n. \tag{2.2}$$

In (2.2), $n > 0$ is a dimensionless parameter and R is the curvature parameter having dimension of a length. Note that the ansatz (2.2) is a generalization of the Finch and Skea [1989] model which can be regained by setting $n = 1$.

We follow the treatment of Maharaj and Maartens [1989] and write the energy-momentum tensor of the anisotropic matter filling the interior of the star in the form

$$T_{ij} = (\rho + p)\, u_i u_j - p g_{ij} + \pi_{ij}, \tag{2.3}$$

where, ρ and p denote the energy-density and isotropic pressure of the fluid, respectively and u_i is the 4-velocity of the fluid. The anisotropic stress-tensor π_{ij} has the form

$$\pi_{ij} = \sqrt{3}S\left[C_i C_j - \frac{1}{3}(u_i u_j - g_{ij})\right], \tag{2.4}$$

where, $C^i = (0, -e^{-\lambda/2}, 0, 0)$. For a spherically symmetric anisotropic distribution, $S(r)$ denotes the magnitude of the anisotropic stress. The non-vanishing components

of the energy-momentum tensor are the following:

$$T_0^0 = \rho, \quad T_1^1 = -\left(p + \frac{2S}{\sqrt{3}}\right), \quad T_2^2 = T_3^3 = -\left(p - \frac{S}{\sqrt{3}}\right). \tag{2.5}$$

Consequently, radial and tangential pressures of the fluid can be obtained as

$$p_r = -T_1^1 = \left(p + \frac{2S}{\sqrt{3}}\right), \tag{2.6}$$

$$p_\perp = -T_2^2 = \left(p - \frac{S}{\sqrt{3}}\right), \tag{2.7}$$

so that

$$S = \frac{p_r - p_\perp}{\sqrt{3}}. \tag{2.8}$$

The potentials of the space-time metric (2.1) and physical variables of the distribution are related through the Einstein's field equations

$$8\pi\rho = \frac{1 - e^{-\lambda}}{r^2} + \frac{e^{-\lambda}\lambda'}{r}, \tag{2.9}$$

$$8\pi p_r = \frac{e^{-\lambda} - 1}{r^2} - \frac{e^{-\lambda}\nu'}{r}, \tag{2.10}$$

$$8\pi p_\perp = e^{-\lambda}\left[\frac{\nu''}{2} + \frac{\nu'^2}{4} - \frac{\nu'\lambda'}{4} + \frac{\nu' - \lambda'}{2r}\right]. \tag{2.11}$$

By defining the mass $m(r)$ within a radius r as

$$m(r) = 4\pi \int_0^r u^2 \rho(u) du, \tag{2.12}$$

we get an equivalent description of the system as

$$e^{-\lambda} = 1 - \frac{2m}{r}, \tag{2.13}$$

$$r(r-2m)\nu' = 8\pi p_r r^3 + 2m, \tag{2.14}$$

$$-\frac{4}{r}(8\pi\sqrt{3}S) = (8\pi\rho + 8\pi p_r)\nu' + 2(8\pi p_r'). \tag{2.15}$$

Using (2.2) in (2.9) and (2.13), we obtain the energy-density and mass $m(r)$ in the form

$$8\pi\rho = \frac{\frac{1}{r^2}\left(1+\frac{r^2}{R^2}\right)\left[\left(1+\frac{r^2}{R^2}\right)^n - 1\right] + \frac{2n}{R^2}}{\left(1+\frac{r^2}{R^2}\right)^{n+1}}, \tag{2.16}$$

$$m(r) = \frac{\frac{r}{2}\left[\left(1+\frac{r^2}{R^2}\right)^n - 1\right]}{\left(1+\frac{r^2}{R^2}\right)^n}. \tag{2.17}$$

To integrate Eq. (2.14), following Sharma and Ratanpal [2013], we write the radial pressure in the form

$$8\pi p_r = \frac{p_0\left(1-\frac{r^2}{R^2}\right)}{R^2\left(1+\frac{r^2}{R^2}\right)^{n+1}}, \tag{2.18}$$

which is a reasonable assumption since the radial pressure vanishes at $r = R$. Consequently, the curvature parameter R in our model turns out to be the boundary of the star. Substituting (2.18) in (2.14) and integrating, we get

$$e^{\nu} = C\left(1+\frac{r^2}{R^2}\right)^{p_0} exp\left[-\frac{p_0 r^2}{2R^2} + \int_0^r \left[\left(1+\frac{u^2}{R^2}\right)^n - 1\right]\frac{1}{u}du\right], \tag{2.19}$$

where, C is a constant of integration.

Finally, using Eqs. (2.15), (2.16) and (2.18), the anisotropy is obtained as

$$8\pi\sqrt{3}S = A_1(r) - \{A_2(r)(A_3(r) + A_4(r))\}, \tag{2.20}$$

where,

$$A_1(r) = \frac{p_0 \frac{r^2}{R^2}\left[(n+2) - \frac{nr^2}{R^2}\right]}{R^2\left(1+\frac{r^2}{R^2}\right)^{n+2}},$$

$$A_2(r) = \frac{1}{4}\left[\left(1+\frac{r^2}{R^2}\right)^{n-1}\right] - \frac{p_0}{4}\frac{r^2}{R^2} + \frac{p_0}{2}\frac{\frac{r^2}{R^2}}{\left(1+\frac{r^2}{R^2}\right)},$$

$$A_3(r) = \frac{\left(1+\frac{r^2}{R^2}\right)\left[\left(1+\frac{r^2}{R^2}\right)^{n} - 1\right]\frac{1}{r^2} + \frac{2n}{R^2}}{\left(1+\frac{r^2}{R^2}\right)^{n+1}},$$

$$A_4(r) = \frac{p_0\left(1-\frac{r^2}{R^2}\right)}{R^2\left(1+\frac{r^2}{R^2}\right)^{n+1}}.$$

Note that the anisotropy vanishes at the center $r = 0$, as expected. Subsequently, the tangential pressure can be obtained from the relation

$$8\pi p_\perp = 8\pi p_r - 8\pi\sqrt{3}S. \tag{2.21}$$

Using the above relations, we also obtain

$$\begin{aligned}
\frac{dp_r}{d\rho} &= \frac{p_0\frac{r^4}{R^4}[(n+2) - n\frac{r^2}{R^2}]}{(1+\frac{r^2}{R^2})^{n+2} - \left[1+\left\{(n+2)+(1-n-2n^2)\frac{r^2}{R^2}\right\}\frac{r^2}{R^2}\right]}, \\
\frac{dp_\perp}{d\rho} &= \frac{1}{c^2}\frac{dp_r}{d\rho} - \frac{p_0\frac{r^4}{R^4}\left[I(r)+D(r)\right] + R^6 B(r)}{4R^6\left(1+\frac{r^2}{R^2}\right)^{n+3}E(r)},
\end{aligned}$$

where,

$$B(r) = F(r) + G(r) + H(r),$$

$$F(r) = \left[\left\{1+\frac{r^2}{R^2}\left(1-n-2n^2\right)\right\}\left(1+\frac{r^2}{R^2}\right)\frac{r^2}{R^2}\right],$$

$$G(r) = \left[1-(n-1)\frac{r^2}{R^2}\right]\left(1+\frac{r^2}{R^2}\right)^{2n+2},$$

$$H(r) = -2\left(1+\frac{r^2}{R^2}\right)^{n+1}\left[1+2\frac{r^2}{R^2} - (n-1)\frac{r^4}{R^4}\right],$$

$$I(r) = 2\left[R^6\left\{\left(1-\frac{3r^2}{R^2}\right)-\left(7-\frac{r^2}{R^2}\right)\frac{nr^2}{R^2} +2\left(1+\frac{r^2}{R^2}\right)^{n+1}\right\}-n^2r^2\left(1-\frac{r^2}{R^2}\right)\right],$$

$$\begin{aligned} D(r) &= -p_0R^6\left(1-\frac{r^2}{R^2}\right) \\ &\quad \left[1-\left\{(n+4)\frac{r^2}{R^2}+(n-1)\frac{r^4}{R^4}\right\}\right], \end{aligned}$$

$$E(r) = \frac{1+(n+2)\frac{r^2}{R^2}-(2n^2+n-1)\frac{r^4}{R^4}}{\left(1+\frac{r^2}{R^2}\right)^{n+2}}-1.$$

Thus, our model has four unknown parameters namely, C, p_0, R and n which can be fixed by the appropriate boundary conditions as will be discussed the following sections.

2.3 Boundary Conditions

At the boundary of the star $r = R$, we match the interior metric (2.1) and (2.2) with the Schwarzschild exterior metric

$$ds^2 = \left(1-\frac{2M}{r}\right)dt^2-\left(1-\frac{2M}{r}\right)^{-1}dr^2-r^2d\theta^2-r^2sin^2\theta\ d\phi^2, \tag{2.22}$$

which yields

$$R = \frac{2^{n+1}M}{2^n-1}, \tag{2.23}$$

$$\begin{aligned} C &= 2^{-(n+p_0)} \\ &\quad exp\left[\frac{p_0}{2}-\int_0^R\left[\left(1+\frac{r^2}{R^2}\right)^n-1\right]\frac{1}{r}dr\right], \end{aligned} \tag{2.24}$$

where $M = m(R)$ denotes the total mass enclosed within a radius R. Eq. (2.23) clearly shows that the compactness of the stellar configuration M/R will depend on the parameter n which was not the case in the model previously developed by Sharma and Ratanpal [2013].

2.4 Bounds on the model parameters

For a physically acceptable stellar model, the following conditions should be satisfied:

(1). $\rho(r) \geq 0, \quad p_r(r) \geq 0, \quad p_\perp(r) \geq 0;$

(2). $\rho(r) - p_r(r) - 2p_\perp(r) \geq 0;$

(3). $\frac{d\rho(r)}{dr} < 0, \quad \frac{dp_r(r)}{dr} < 0, \quad \frac{dp_\perp(r)}{dr} < 0;$

(4). $0 \leq \frac{dp_r}{d\rho} \leq 1, \quad 0 \leq \frac{dp_\perp}{d\rho} \leq 1.$

Due to mathematical complexity, it is difficult to show analytically that our model complies with all the above mentioned conditions. However, by adopting numerical procedures, we have shown that for a specified bound all the above requirements can be fulfilled in this model.

Now, to get an estimate on the bounds of the model parameters, we note that $p_r,\ p_\perp \geq 0$ at $r = R$ if we have

$$p_0 \leq \frac{(2^n - 1)(2^n - 1 + n)}{2}. \tag{2.25}$$

The strong energy condition $\rho - p_r - 2p_\perp \geq 0$ at $r = R$ puts a further constraint on the parameter p_0 given by

$$p_0 \geq \frac{3(1-n)}{2} + (n - 4 + 2^n)2^{n-1}. \tag{2.26}$$

The condition $\frac{dp_\perp}{dr} \mid_{r=R} < 0$ imposes the following constraint on p_0

$$p_0 > \frac{\left(n^2 - 2\left(2^n - 1\right)^2 + 2^n n\left(2^n - 1\right)\right)}{(2 - 3n + 2^{n+1})}. \tag{2.27}$$

The requirement $\frac{dp_\perp}{d\rho} \mid_{r=R} < 1$ puts the following bound

$$p_0 < 2^{n+1} + n^2 - 2. \tag{2.28}$$

Similarly, the conditions $\frac{dp_\perp}{d\rho} \mid_{r=0} < 1$ and $\frac{dp_\perp}{d\rho} \mid_{r=R} < 1$, respectively put the following constraints on p_0:

$$p_0 < 8 + 2n - \sqrt{64 + 22n - 9n^2}, \tag{2.29}$$

$$p_0 < \frac{4(2^{n+1} + n^2 - 2) - 2(2^n - 1)^2 + 2^n(2^n - 1) + n^2}{2^{n+1} - 3n + 2}. \tag{2.30}$$

All the above constraints when put together provide an effective bound

$$\frac{n^2 - 2\left(2^n - 1\right)^2 + 2^n n\left(2^n - 1\right)}{2 - 3n + 2^{n+1}} < p_0 \leq \frac{(2^n - 1)(2^n - 1 + n)}{2} \tag{2.31}$$

on p_0 and n.

2.4.1 Stability

Though we have obtained an effective bound on p_0 and n based on requirements (i)-(iv), a more stringent bound on these parameters may be obtained by analyzing the stability of the system. To check stability, we have followed the method of Herrera et al. [1992] which states that for a potential stable configuration we should have $(\upsilon_\perp^2 - \upsilon_r^2) \mid_{r=0} < 0$. In our case, the difference between the radial speed of sound $\upsilon_r^2 (= \frac{dp_r}{d\rho})$ and tangential speed of sound $\upsilon_\perp^2 (= \frac{dp_\perp}{d\rho})$ evaluated at the centre $r = 0$ is

obtained as

$$(\upsilon_{\perp}^2 - \upsilon_r^2)\mid_{r=0} = -\frac{3n^2 + (p_0 - 8)\, p_0}{10n(n+1)}. \tag{2.32}$$

Then Herrera's stability condition implies

$$p_0 < 4 - \sqrt{16 - 3n^2}. \tag{2.33}$$

Similarly, $(\upsilon_{\perp}^2 - \upsilon_r^2)\mid_{r=R} < 0$ yields

$$p_0 < n^2 - 2^n(n-4) + 4^n(n-2) - 2. \tag{2.34}$$

Combining (2.31), (2.33) and (2.34), the most appropriate bound on the model parameters is finally obtained in the form

$$\frac{n^2 - 2\left(2^n - 1\right)^2 + 2^n n\left(2^n - 1\right)}{2 - 3n + 2^{n+1}} < p_0 < 4 - \sqrt{16 - 3n^2}. \tag{2.35}$$

It is to be noted that for a real valued upper bound on p_0 we must have $n \leq \frac{4}{\sqrt{3}}$. In Fig. 2.1, we have shown the possible range of p_0 and n (shaded region) for which a physically acceptable stable stellar configuration is possible.

2.5 Physical analysis

Having derived a physically plausible model, let us now analyze the implications of the modified Finch and Skea [1989] ansatz. Note that in our description, two of the four unknown parameters can be determined from the boundary conditions (2.23) and (2.25) provided the mass is known. Since the condition $p_r(R) = 0$ is automatically satisfied, it provides no additional information about the unknowns. Therefore, n and p_0 remain free parameters in our construction. For a chosen value

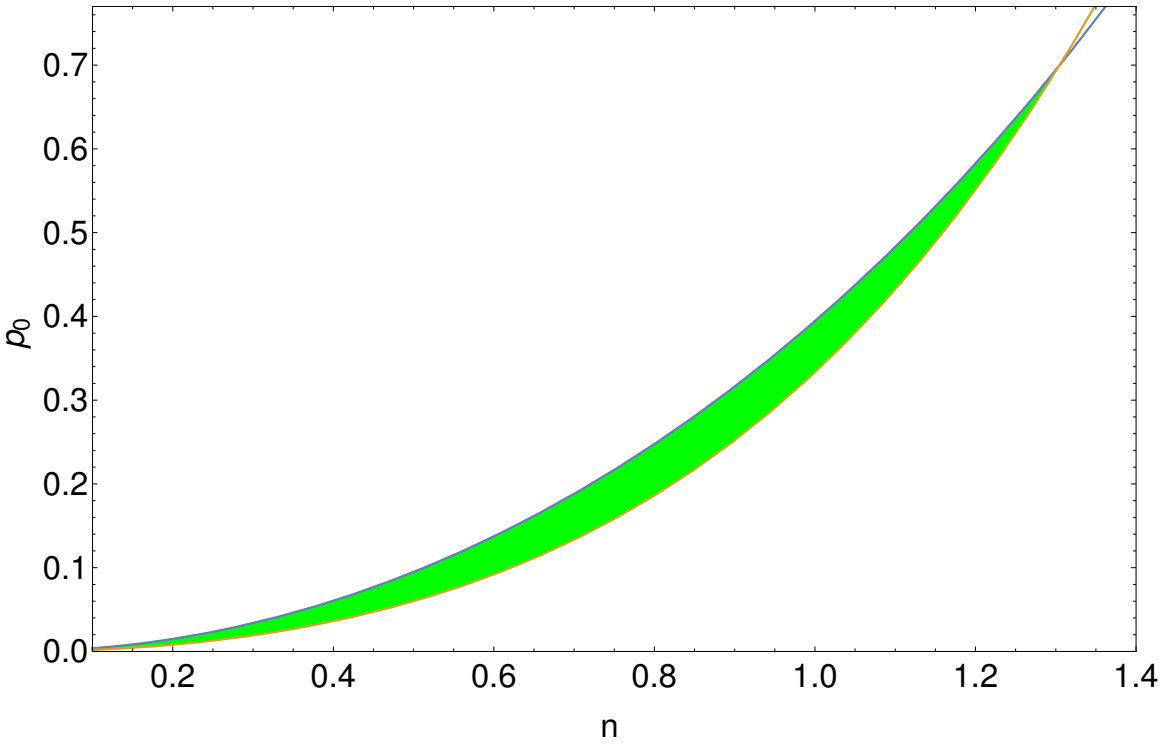

Figure 2.1: Bounds on the model parameters p_0 and n based on physical requirements and stability.

of n, the parameter p_0 can be appropriately fixed from within the bound provided in (2.35). Thus, all the physically interesting quantities of the model can be evaluated if the mass M is supplied.

To examine the nature of physical quantities, we have considered the pulsar $4U1820-30$ whose estimated mass and radius are given by $M = 1.58\ M_{\odot}$ and $R = 9.1$ km, respectively [Güver et al., 2010a]). Assuming $M = 1.58\ M_{\odot}$, we note that if we set the dimensionless parameter $n = 0.6154$ and $p_0 = 0.1211$ Mev fm^{-3}, we get exactly the same radius as estimated by Güver et al. [2010a]. Moreover, the compactness of the star can be made as high as ~ 0.4543 for an upper limit of $n \sim 1.38$. Similarly, we have considered some other well studied pulsars like PSR J1903+327 [*et al*, 2011]), 4U 1608-52 and Vela X-1 [Rawls et al., 2011]), PSR J1614-2230 [Demorest et al., 2010]), SAX J1808.4-3658 [Elebert et al., 2009]) and Her X-1 [Abubekerov et al., 2008]) and shown that the estimated masses and radii of these stars can also

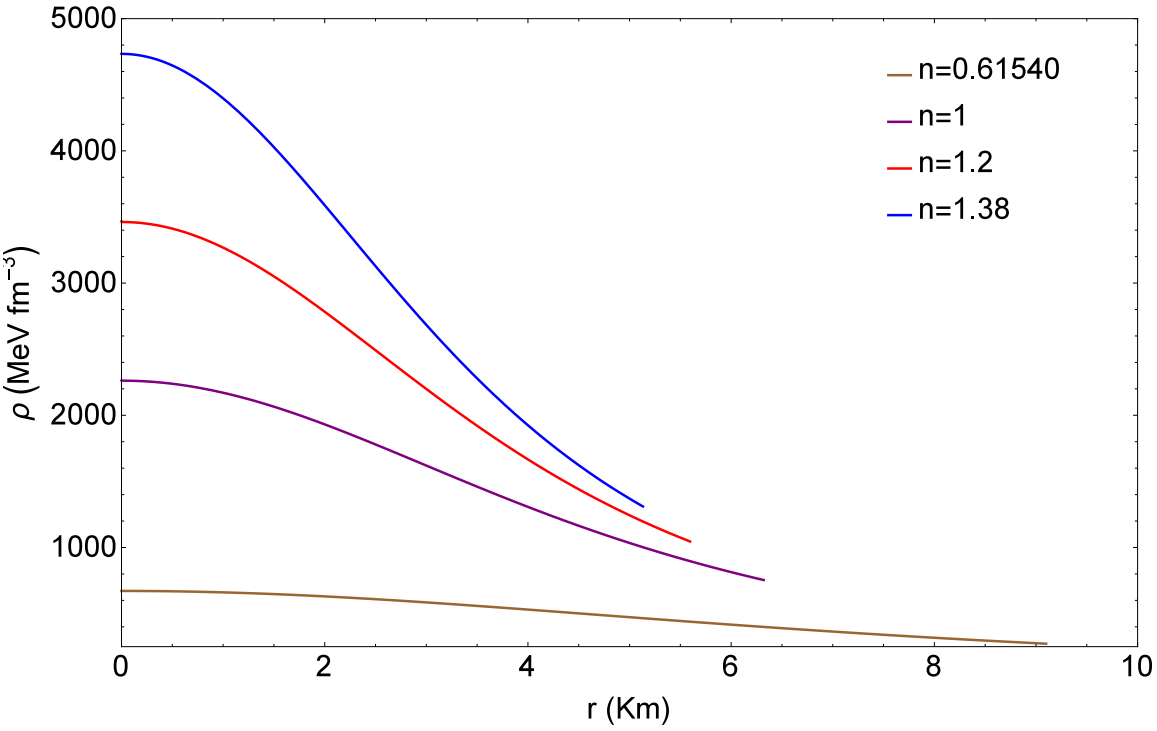

Figure 2.2: Variation of density (ρ) against the radial parameter r.

be obtained by making necessary adjustments in the values of n. In Table 2.1, we have given the appropriate values of the adjustable *compactness parameter* u for which one can obtain the predicted masses and radii of the stars considered here. Respective central density (ρ_0), surface density (ρ_R), central pressure (p_{r0}) and compactness ($u = \frac{M}{R}$) have also been shown in the table. The difference in the values of these parameters for different choices of n has also been shown.

For a particular mass $M = 1.58\ M_\odot$, we have also shown that all the physical quantities are well behaved at all interior points of the star within the specified bounds on n and p_0. In Fig. 2.2, we have shown the variation of density which shows that the density decreases from its maximum value at the centre towards the boundary. Moreover, the central density increases if the value of n increases. In Fig. 2.3, radial variation of the two pressures has been shown. As expected, the

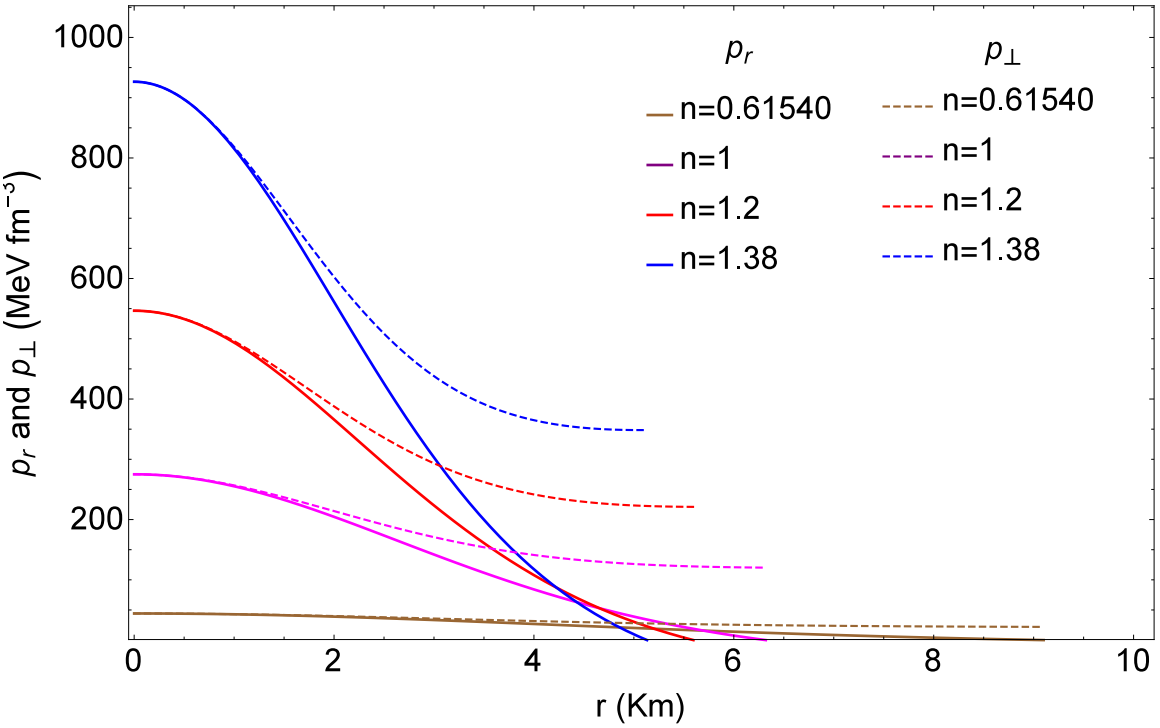

Figure 2.3: Variation of radial (p_r) and transverse ($p_\perp$) pressure against the radial parameter r.

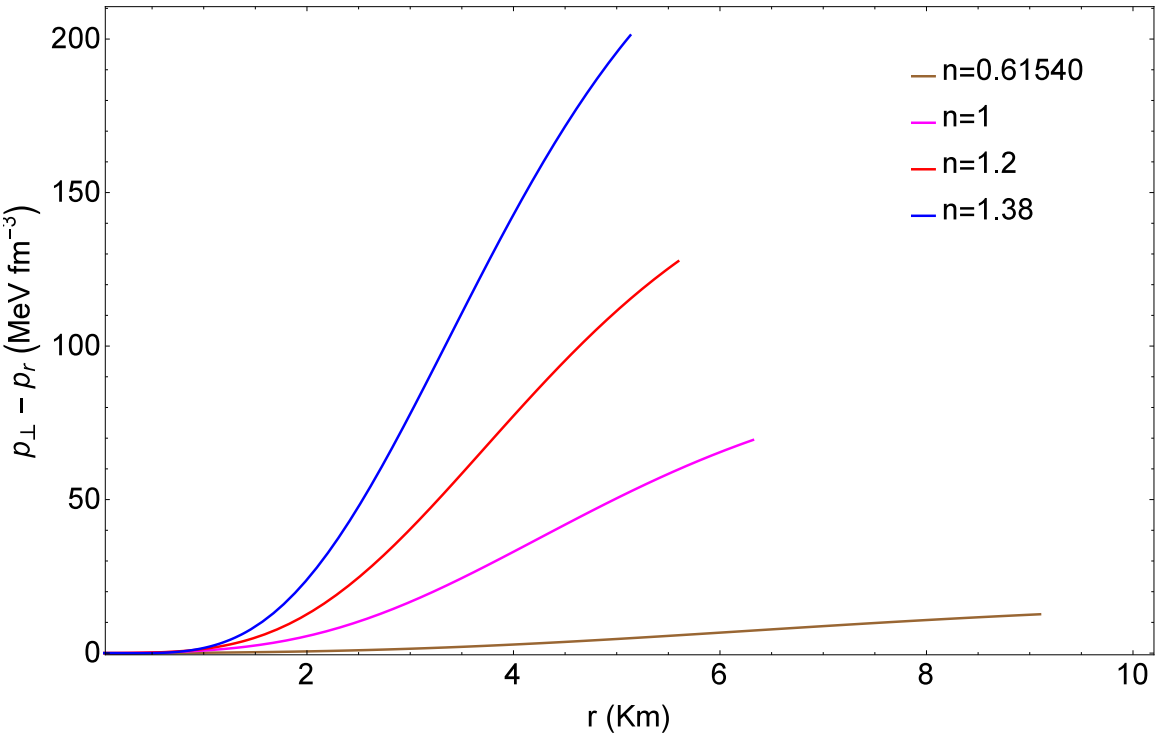

Figure 2.4: Variation of anisotropy ($p_\perp - p_r$) against r.

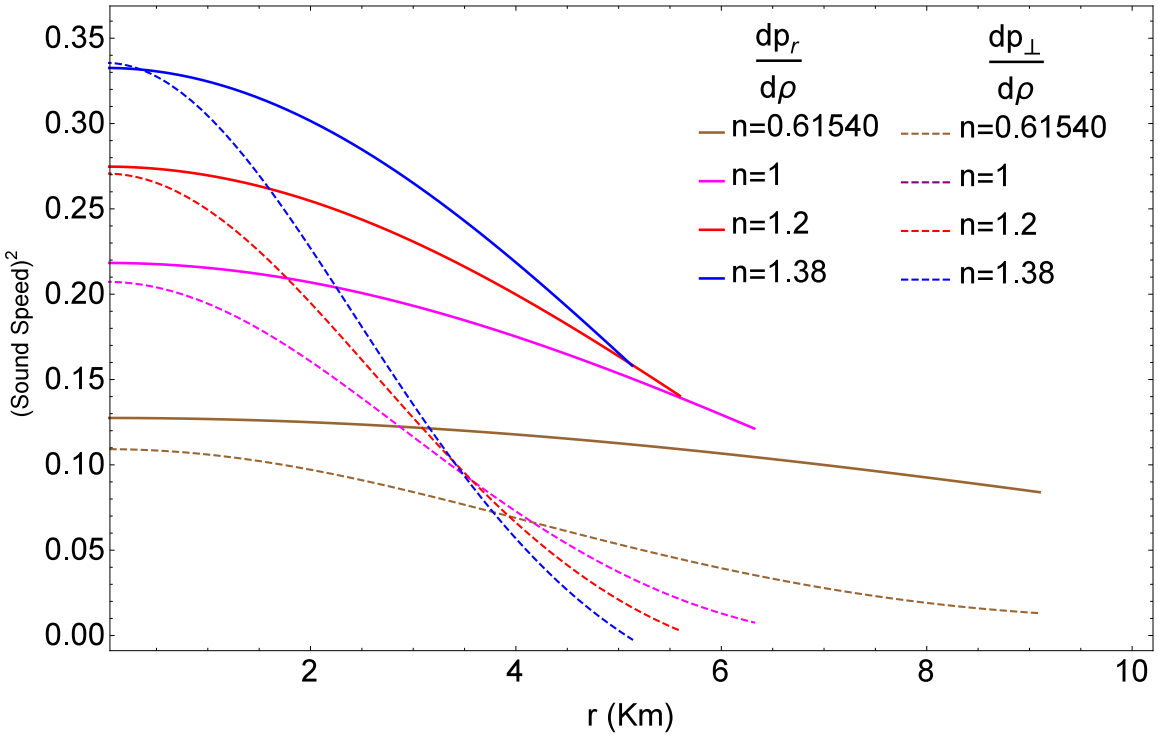

Figure 2.5: Variation of $\frac{dp_r}{d\rho}$ and $\frac{dp_\perp}{d\rho}$ against the radial parameter r.

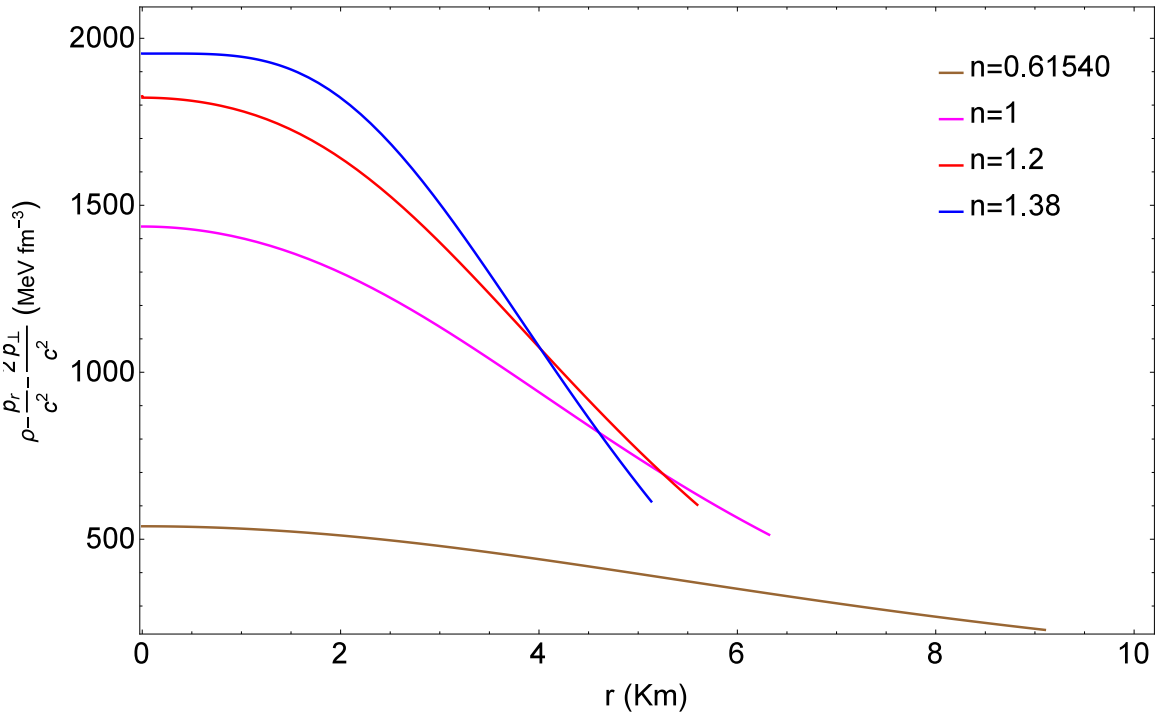

Figure 2.6: $(\rho - p_r - 2p_\perp)$ plotted against the radial parameter r.

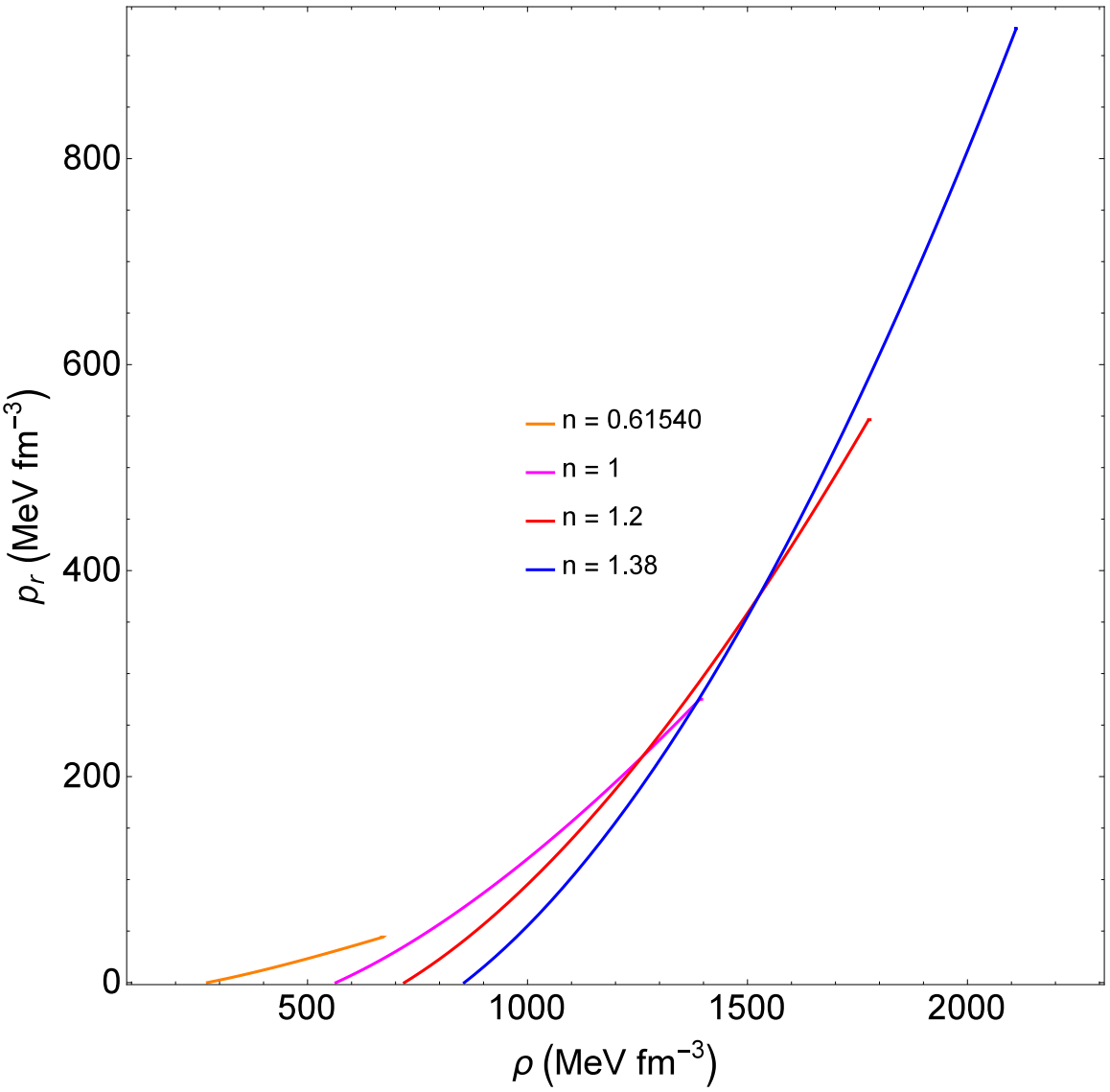

Figure 2.7: Variation of radial pressure (p_r) against density (ρ)

Table 2.1: Estimation of physical values based on observational data.

STAR	n	p_{r0} MeV fm^{-3}	M $M_\odot$	R (Km)	ρ_c MeV fm^{-3}	ρ_R MeV fm^{-3}	$u(=\frac{M}{R})$	$\left(\frac{dp_r}{d\rho}\right)_{r=0}$
4U 1820-30	**0.6154**	**0.1211**	**1.58**	**9.1**	**671.36**	**272.35**	**0.2561**	**0.1275**
	1	0.3638		6.32	2261.77	753.93	0.3688	0.2183
	1.2	0.5667		5.59	3469.29	1047.59	0.4169	0.2748
	1.38	0.8079		5.13	4737.27	1311.33	0.4543	0.3326
PSR J1903+327	**0.6287**	**0.1269**	**1.667**	**9.438**	**637.65**	**256.89**	**0.2605**	**0.1303**
	1	0.3638		6.66	2036.74	678.91	0.3692	0.2183
	1.2	0.5667		5.90	3114.30	940.39	0.4168	0.2748
	1.38	0.8079		5.41	4259.59	1179.11	0.4545	0.3326
4U 1608-52	**0.6752**	**0.1485**	**1.74**	**9.31**	**703.83**	**276.78**	**0.2757**	**0.1405**
	1	0.3638		6.96	1864.94	621.65	0.3688	0.2183
	1.2	0.5667		6.16	2856.95	862.69	0.4166	0.2748
	1.38	0.8079		5.65	3905.40	1081.06	0.4542	0.3326
Vela X-1	**0.6672**	**0.1446**	**1.77**	**9.56**	**659.553**	**260.45**	**0.2731**	**0.1387**
	1	0.3638		7.08	1802.26	600.75	0.3688	0.2183
	1.2	0.5667		6.27	2757.59	832.68	0.4164	0.2748
	1.38	0.8079		5.75	3770.74	1043.79	0.4540	0.3326
PSR J1614-2230	**0.7529**	**0.1892**	**1.97**	**9.69**	**724.42**	**273.692**	**0.2999**	**0.1578**
	1	0.3638		7.88	1454.89	484.96	0.3688	0.2183
	1.2	0.5667		6.98	2225.12	671.90	0.4163	0.2748
	1.38	0.8079		6.40	3043.71	842.54	0.4540	0.3326
SAX J1808.4-3658	**0.3703**	**0.0411**	**0.9**	**7.951**	**529.18**	**244.30**	**0.1669**	**0.0768**
	1	0.3638		3.6	6970.73	2323.58	0.3688	0.2183
	1.2	0.5667		3.19	10653.30	3216.86	0.4161	0.2748
	1.38	0.8079		2.92	14621.70	4047.46	0.4546	0.3326
Her X-1	**0.3399**	**0.0344**	**0.85**	**8.1**	**467.95**	**219.575**	**0.1548**	**0.1031**
	1	0.3638		3.40	7814.94	2604.98	0.3688	0.2183
	1.2	0.5667		3.01	11965.50	3613.11	0.4165	0.2748
	1.38	0.8079		2.76	16366.1	4530.33	0.4543	0.3326

radial pressure p_r vanishes at the boundary; however the tangential pressure $p_\perp$ remains finite at the boundary. As in the case of density, both pressures increase as n increases. In Fig. 2.4, radial variation of anisotropy has been shown which shows that anisotropy is zero at the centre and is maximum at the surface. In Fig. 2.5, radial variations of sound speed in the radial and transverse directions have been shown which confirms that the causality condition is not violated throughout the configuration. In Fig. 2.6, we have plotted $(\rho - p_r - 2p_\perp)$ which was shown to remain positive thereby implying that the strong energy condition is not violated in this model. Though we have not assumed any explicit EOS in our model, Fig. 2.7 shows how the radial pressure varies against the density for different values of n.

2.6 Discussion

In this chapter, we have solved the Einstein's field equations describing a spherically symmetric anisotropic matter composition by assuming the form of one of the metric potentials of the associated space-time and also by choosing a particular radial pressure profile. The assumed form of the metric potential is a generalization of the Finch and Skea [1989] ansatz, which has so far been utilized successfully by many authors to generate solutions to the Einstein's field equations in different astrophysical contexts. We note that a modification of the Finch and Skea [1989] ansatz for the metric potential g_{rr} allows us to fit the theoretically obtained compactness to the observed compactness of a given star. We have shown that in the presence of such an adjustable parameter, it is possible to accommodate a large class of observed pulsars in our model. Another interesting feature of our approach is that though no a priori knowledge of the EOS is required in our set up, we have been able to show that the predicted masses and radii of the pulsars based on the exotic strange matter EOS formulated by Dey et al. [1998] and examined by Gangopadhyay et al. [2013] can also be fitted into our model.